ICARUS **134,** 292–302 (1998)
ARTICLE NO. IS985961

Radar Detectability of a Subsurface Ocean on Europa

Christopher F. Chyba[1]

Lunar and Planetary Laboratory, University of Arizona, Tucson, Arizona 85721-0092
E-mail: chyba@lpl.arizona.edu

Steven J. Ostro

Jet Propulsion Laboratory, California Institute of Technology, MS 300-233, Pasadena, California 91109-8099

and

Bradley C. Edwards

Los Alamos National Laboratory, MS D436, Los Alamos, New Mexico 87544

Received October 9, 1997; revised May 5, 1998

A spacecraft in orbit around Jupiter's moon Europa can use ice penetrating radar to probe for a possible liquid water ocean beneath Europa's surface ice and to characterize other important subsurface structure. Consideration of available constraints on the properties of Europa's ice, possible subsurface temperature gradients, and possible impurities in the ice places an upper limit of about 10 km on the depth to which an ocean might be detectable with an orbiting radar.

I. INTRODUCTION

The initial reconnaissance of the jovian system by the Voyager spacecraft (Smith *et al.* 1979a,b, Malin and Pieri 1986) and models of tidal heating of natural satellites suggested the possibility of a liquid water ocean beneath the ice of Jupiter's moon Europa (Cassen *et al.* 1979, 1980, 1982, Squyres *et al.* 1983, Ross and Schubert 1987, Ojakangas and Stevenson 1989). Recent high resolution imaging of Europa from the Galileo spacecraft (Belton *et al.* 1996, McKinnon 1997a, Carr *et al.* 1998) is consistent with this interpretation, and suggests that in some locations, liquid water may lie within a few kilometers or less of Europa's surface. Since liquid water is essential for life as we know it, the possible existence of a second liquid water ocean in the Solar System is of great exobiological interest (Reynolds *et al.* 1983, 1987, Chyba and McDonald 1995). In addition, a subsurface Europan ocean may provide a model for early Earth at the time of the terrestrial origin of life (Bada *et al.* 1994). The search for and initial characterization of a Europan ocean via an orbiting spacecraft is now one of the highest priority objectives of Solar System exploration.

It has been suggested (Squyres 1989) that an orbiting radar sounder might be able to detect the presence of a subsurface Europan ocean. The radar detectability of the putative ocean depends on the transparency of the overlying ice, which in turn will depend on the ice's purity and temperature gradient, as well as the radar wavelength. Here we demonstrate that consideration of those factors plus available constraints on the properties of Europan ice places a limit of about 10 km on the depth to which an ocean might be detectable with an orbiting radar.

II. PREVIOUS RADAR OBSERVATIONS

Extensive radar sounding of Greenland and polar ice sheets, sea ice, and glaciers provides a baseline of terrestrial experience (Evans and Smith 1969, Gudmandsen 1971, Drewry 1981, Robin *et al.* 1983, Daniels *et al.* 1988, Fisher *et al.* 1989, Hallikainen and Winebrenner 1992, Kovacs and Morey 1992). Terrestrial ice-covered lakes (Oswald and Robin 1973, Oswald 1975), such as Lake Vostok in Antarctica (Kapitsa *et al.* 1996), have been detected and characterized beneath as much as 4 km of polar ice. It is easier to sound colder (polar) ice than warmer (temperate glacier or sea) ice, in part because attenuation in ice decreases exponentially with decreasing temperature (Evans 1965, Hobbs 1974). This suggests that, all else being equal, it

[1] Present address: SETI Institute, 2035 Landings Drive, Mountain View, CA 94043, and Department of Geological and Environmental Sciences, Stanford University, Palo Alto, CA 94305-2115.

0019-1035/98 $25.00

may be possible to penetrate much deeper into Europan ice (with surface temperatures ~100 K) than in the terrestrial analogs.

Warm terrestrial ice contains pockets of liquid water or brines that serve as powerful scattering centers (Paterson and Savage 1970, Strangway *et al.* 1974, Watts and England 1976), an impediment that may exist near a Europan ice/water interface. Interstitial brines within warm ice might also lead to substantial conduction losses. For plausible salts that may be present in high concentrations in Europan water, temperatures below about 210–220 K (depending on depth) will lead to complete freezing (Kargel 1991), so that liquid brines are expected only in the warm ice approaching the putative ice/water interface. However, if recently suggested models (Pappalardo *et al.* 1998) of solid-state convection in Europa's ice shell were correct, temperatures permissive of liquid brines might extend from the putative ocean up to nearly the bottom of a brittle lithosphere ice layer less than 2 km thick. Given the possible salt content of a Europan ocean (McCord *et al.* 1998), there may be a temperature limit well below 273 K above which a warm convecting "ice" layer may simply become a liquid briny water layer.

Earth-based radar observations of Europa at 3.5 and 13 cm (Ostro 1982, Ostro *et al.* 1992) show that Europa's average total-power radar albedo (2.7) exceeds that of any other radar-detected Solar System object (e.g., the Moon's albedo is 0.1). The ratio of echo power in the same sense of circular polarization as transmitted to the opposite sense is higher for Europa (1.6) than for any other target (again, the lunar value is 0.1). This implies that the uppermost 10 m or more of Europa's surface are very clean ice possessing density variations at scales that multiply scatter 3.5- to 13-cm waves (Ostro and Shoemaker 1990). At 70 cm, Europa's albedo drops by at least an order of magnitude (Black *et al.* 1996). This suggests either that scattering centers disappear below ~10 m depth, or that there is a cutoff in the size of the scattering centers that reduces their scattering efficiency at longer wavelengths. In either case, deeper penetration into the ice is evidently possible at wavelengths beyond ~1 m. At the same time, decametric radiation (noise) from Jupiter increases rapidly at frequencies below about 50 MHz, increasing by some 6 orders of magnitude by 10 MHz (Carr *et al.* 1983), requiring that radar observations not shielded by the body of Europa be done at wavelengths shorter than ~10 m.

III. TEMPERATURE DEPENDENCE OF RADAR ATTENUATION IN ICE

Attenuation α (measured in decibels per meter) of electromagnetic wave power in ice is given by (Evans 1965, Gudmansen 1971)

$$\begin{aligned}\alpha &= 0.129\sqrt{\varepsilon_r}\,\nu[\sqrt{(1+\tan^2\delta)}-1]^{1/2}\ \text{dB/m}\\ &\approx 0.091\sqrt{\varepsilon_r}\,\nu\tan\delta\ \text{dB/m},\end{aligned} \tag{1}$$

where the loss tangent $\tan\delta = \varepsilon_i/\varepsilon_r$, ε_r and ε_i are the real and imaginary parts of the dielectric constant (permittivity), ν is the frequency in MHz, and the second equality holds for $\tan\delta \ll 1$. Data for ice at temperatures ranging from −1 to −60°C over the frequency range 1 mm to 10 m (Warren 1984) show that attenuation increases dramatically at wavelengths shorter than ~1 m, but remains flat beyond 1 m.

Earth-based sounding of Europa, jovian decametric radiation, and the attenuation properties of ice all suggest wavelengths of several meters as the best choice for ice sounding at Europa. For definiteness, calculations in this paper are done using a free-space wavelength of 6 m (50 MHz). Given uncertainties over what will be found at Europa, a frequency-agile system capable of sounding at more than one wavelength in the meter to tens-of-meters range would seem a wise choice for an actual flight system.

We interpolate experimental data (Johari and Charette 1975) for attenuation in ice at 35 MHz (8.6 m) and 60 MHz (5 m) to 50 MHz (6 m) and extrapolate to Europan temperatures (surface temperatures ~50–100 K). This requires modeling how permittivities vary with temperature. For a regular dielectric such as ice, ε_r and ε_i vary with temperature T and circular frequency $\omega = 2\pi\nu$ according to the Debye equation. ε_r and ε_i are given by

$$\varepsilon_r = \varepsilon_\infty + (\varepsilon_0 - \varepsilon_\infty)/(1+\omega^2\tau^2), \tag{2a}$$

and

$$\varepsilon_i = \omega\tau(\varepsilon_0 - \varepsilon_\infty)/(1+\omega^2\tau^2), \tag{2b}$$

where τ is the dielectric relaxation time, ε_0 the low-frequency (compared with τ^{-1}) permittivity, and ε_∞ the high-frequency permittivity (Evans 1965, Hobbs 1974).

Both τ and $(\varepsilon_0 - \varepsilon_\infty)$ are temperature dependent. Since an ordered orientation of the molecular dipoles in the dielectric is resisted by thermal agitation, a Boltzmann principle applies and

$$\tau = C\exp(E/k_B T), \tag{3a}$$

where $C = 5.30 \times 10^{-16}$ s, the activation energy $E = 0.571$ eV (Hobbs 1974), and $k_B = 8.61 \times 10^{-5}$ eV K^{-1} is the Boltzmann constant, so that $\tau = C\exp(6629/T)$. The high-frequency permittivity ε_∞ has a slight dependence on T that is well approximated as linear (Gough 1972, Hobbs 1974, Mätzler and Wegmüller 1987). For the parameters adopted here,

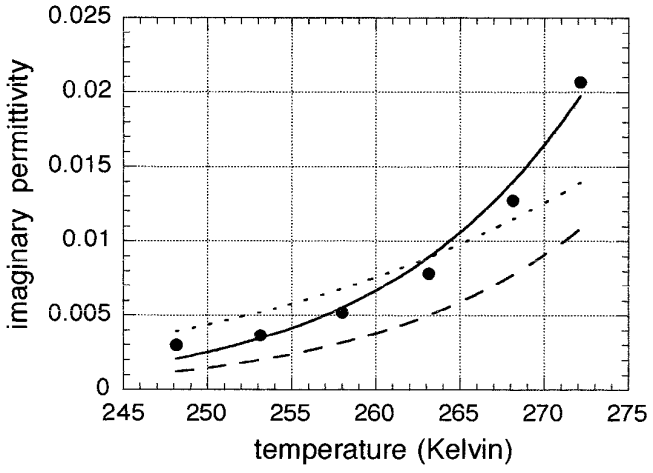

FIG. 1. The imaginary part of the dielectric constant of ice vs temperature, for laboratory measurements at 60 MHz (Johari and Charette 1975) and several ice attenuation models. The dots indicate laboratory data; error bars are smaller than the plotted dot size. The solid line is a fit to the data using the Debye equations, Eqs. (2), and the parameter choices explained in the text (Eqs. (3)). This fit is used in the modeling presented in this paper. The dashed and dotted lines correspond to best fits using the models (Thompson and Squyres 1990) presented as Eqs. (4) and (5), respectively.

$$\varepsilon_\infty = 3.02 + 6.41 \times 10^{-4}\, T. \tag{3b}$$

The difference $\varepsilon_0 - \varepsilon_\infty$ obeys the Curie–Weiss law:

$$\varepsilon_0 = \varepsilon_\infty + A_c/(T - T_c); \tag{3c}$$

where $T_c \approx 35$ K (Hobbs 1974). Values for T_c ranging from 15 K (Johari and Jones 1978) to 46 K (Kawada 1978) may be found in the literature. We determine A_c by fitting Eq. (2b) as a function of temperature to experimental data at 5 and 8.6 m over the temperature range 272 to 248 K (Johari and Charette 1975) interpolated to 6 m. These data are well-fit (Fig. 1) when $A_c = 3.54 \times 10^4$ K, a value within the scatter of other determinations of A_c (Hobbs 1974). The resulting formulae for ε_r and ε_i as a function of temperature T may then be used in Eq. (1), allowing the extrapolation of attenuation in ice to lower temperatures.

Thompson and Squyres (1990) have proposed two different fits to experimental data for dielectric attenuation in ice. They suggest extrapolating to shorter wavelengths the fit by Johari and Jones (1978) to those authors' data in the temperature range 270 to 200 K at wavelengths beyond 1.5 km. This gives

$$\tau = 9.3 \times 10^{-13}\, T^{-1} \exp(6150/T)\ \text{s}, \tag{4a}$$

$$\varepsilon_\infty = 3.083 + 2.8 \times 10^{-4}\, T, \tag{4b}$$

and

$$\varepsilon_0 = \varepsilon_\infty + 23400/(T - 15) \tag{4c}$$

as values to be used in Eqs. (2) for ε_i and ε_r.

In addition, Thompson and Squyres (1990) empirically fit data summarized by Warren (1984) from many different experimenters over the wavelength range 1 mm to 8.6 m and temperatures from 213 to 272 K. Their empirical fit is:

$$\varepsilon_i = (\varepsilon_D^3 + \varepsilon_S^3)^{1/3}, \tag{5a}$$

with

$$\log(\varepsilon_S) = -0.627 - 434.5/T - 0.742 \log \lambda, \tag{5b}$$

and

$$\log(\varepsilon_D) = 1.13 - 1547/T + \log \lambda, \tag{5c}$$

where λ is the free-space wavelength.

The three fits considered here, Eqs. (3), (4), and (5), are evaluated at 60 MHz and compared to laboratory data (Johari and Charette 1975) at this frequency in Fig. 1. Comparison to data at 35 MHz gives nearly identical results. These data are identified as the most relevant to the modeling pursued here as both frequencies lie in the range relevant to radar sounding at Europa, and bracket the 50-MHz frequency employed in this paper. As can be seen in Fig. 1, Eqs. (3) provide a superior fit to these data. Equations (3) will therefore be used throughout the modeling reported here.

Nevertheless, a legitimate cause for concern is the limited temperature range over which the data in Fig. 1 extend. Estimates of ε_i at temperatures extending down to ~80 K at $\lambda = 1.25$ cm (Lamb and Turney 1949) or $\lambda > 3$ km (Gough 1972) suggests that Eqs. (3) may significantly underestimate attenuation at low temperatures. Fits to data in the 10^{-3} Hz to 5 k Hz range suggest that the ice activation energy drops from 0.57 to 0.23 eV at temperatures below 220 K (Kawada 1978), suggesting that Eqs. (3) may greatly underestimate ε_i at low temperatures in at least this frequency range.

Ultimately these concerns should be addressed through a systematic set of experiments at wavelengths in the range 1 to 10 m and at temperatures from 273 to 50 K, allowing a better empirical fit to the parameters in Eqs. (3). Until such results become available, however, we may rely on

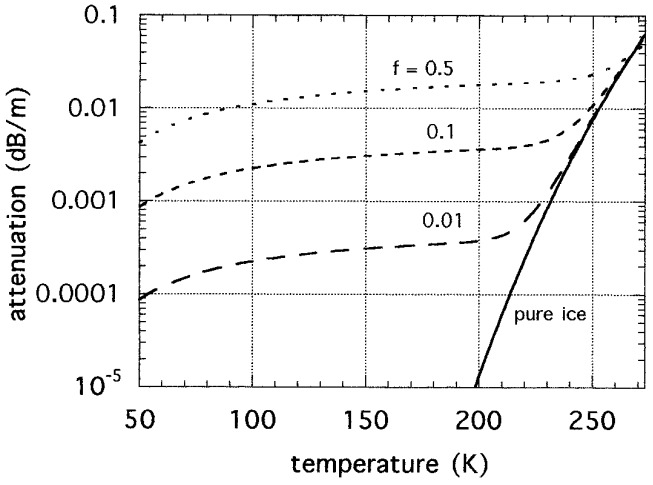

FIG. 2. Absorption at 50 MHz in dirty ice as a function of temperature and impurity content. The solid line shows attenuation (dB/m) in pure ice; the dashed lines show attenuations for ice with lunar soil (Eq. (6)) mixed in according to Eq. (2) for (from bottom to top) mixing fractions $f = 0.01$, 0.1, and 0.5. Attenuation in lunar soil is dominated by the soil's metallic content.

the result that, as shown in Fig. 2, attenuation in pure ice falls so quickly with temperature that the details of attenuation in ice below ~200 K are likely to be unimportant compared with the effects of contaminants. For impurity concentrations above ~1%, dielectric absorption by ice becomes unimportant at temperatures below ~210 K, because the impurities dominate absorption. Similarly, at impurity concentrations ~10%, absorption in ice becomes unimportant at temperatures below ~230 K.

IV. EFFECT OF IMPURITIES IN THE ICE

Impurities in Europan ice could strongly affect a radar sounding experiment. We therefore consider the radar attenuation caused by mixing different impurities into an ice matrix. There is a large body of work on the dielectric properties of mixtures; here we employ the Rayleigh mixing formula, which holds for spherical scatterers of permittivity ε_s and diameters $d_s \leq \lambda/2\pi$, embedded in a background medium (ice) of permittivity ε. The effective permittivity ε_{eff} is then (Nielsen 1978, Sihvola and Kong 1988, 1989)

$$\varepsilon_{\text{eff}} = \varepsilon + 3f\varepsilon(\varepsilon_s - \varepsilon)/[(1+f)\varepsilon_s + (2+f)\varepsilon], \quad (6)$$

where f is the fractional volume occupied by the scatterers. The real and imaginary parts of Eq. (6) are

$$\varepsilon_{\text{eff,r}} = \varepsilon_r + 3f(ac + bd)/(c^2 + d^2) \quad (7a)$$

and

$$\varepsilon_{\text{eff,i}} = \varepsilon_i + 3f(bc - ad)/(c^2 + d^2), \quad (7b)$$

with

$$a = \varepsilon_i^2 - \varepsilon_r^2 + \varepsilon_r\varepsilon_{s,r} - \varepsilon_i\varepsilon_{s,i}, \quad (7c)$$

$$b = \varepsilon_r\varepsilon_{s,i} - 2\varepsilon_i\varepsilon_r + \varepsilon_i\varepsilon_{s,r}, \quad (7d)$$

$$c = \varepsilon_{s,r}(1-f) + \varepsilon_r(2+f), \quad (7e)$$

and

$$d = \varepsilon_{s,i}(1-f) + \varepsilon_i(2+f). \quad (7f)$$

We then calculate attenuation α by using Eqs. (7) in Eq. (1).

We use the attenuation properties of lunar samples to provide a model impurity to mix in with Europa's ice. As will be seen below, attenuation by lunar samples is dominated by incorporated metals. Olhoeft and Strangway (1975) have reviewed 92 measurements of lunar rock and soil samples, and find by regression analysis that the real part of ε_s is given by

$$\varepsilon_{s,r} = (1.93 \pm 0.17)^{\rho}, \quad (8)$$

where ρ is the sample density in g cm^{-3} and the equation holds for frequencies above 100 kHz. Similarly, the loss tangent is

$$\tan\delta_s = [(0.00053 \pm 0.00056) + (0.00025 \pm 0.00009)C]\rho, \quad (9)$$

where C is the percentage of FeO + TiO_2 (primarily metallic ilmenite) in the sample. The average percentages of TiO_2 and FeO in lunar samples are 3.3 ± 3.6% and 12.9 ± 6.3%, respectively (Olhoeft and Strangway 1975). The corresponding abundances for carbonaceous chondrites (types I, II, and III) are 0.1 ± 0.03 and 17.2 ± 7.7%, respectively (Wiik 1956), so $C = 16$ is a representative choice for nonterrestrial Solar System materials. The loss tangent is dominated by FeO, which accounts for ~75% of the total attenuation.

At frequencies above 100 kHz, the frequency dependence of $\varepsilon_{s,r}$ is negligible, as is the temperature dependence for $T < 300$ K (Saint-Amant and Strangway 1970, Olhoeft *et al.* 1974). The loss tangent, however, has weak frequency and temperature dependencies, which vary significantly from sample to sample (Chung *et al.* 1972, Chung and Westphal 1973, Bussey 1979). An analytical fit has been derived for lunar soil sample 15301,38 (Olhoeft *et al.* 1974); to a good approximation $\tan\delta_s \propto \omega^{-\beta}$ where $\beta = 0.33$. Most measurements contributing to Eq. (9) were made in the range 10^5 to 4.5×10^8 Hz; here we assume Eq. (9) to hold at 50 MHz.

The temperature dependence of tan δ varies substantially between lunar rock samples. At 10 MHz, tan δ is typically ~1 order of magnitude lower at 77 K than at 475 K (Chung *et al.* 1972, Chung and Westphal 1973). Data for the temperature dependence of lunar soil sample 15301,38 in the range 298 to 973 K has been fit (Olhoeft *et al.* 1974) with the analytical formula

$$\tan \delta_s \propto \exp(-\beta E_0/k_B T), \tag{10}$$

where the activation energy $E_0 = 0.025$ eV (or less; we adopt this value). Equation (9) was determined for $T = 298$ K; we extrapolate to lower temperatures according to Eq. (10). From 273 to 50 K, tan δ varies by a factor of 5, dropping from 6×10^{-3} to 1×10^{-3}. Loss tangents for lunar rocks measured at 10 MHz over the range 273 to 77 typically vary from $\sim 10^{-2}$ to $\sim 10^{-3}$, respectively, consistent with this extrapolation.

A typical lunar surface density (Olhoeft and Strangway 1975) is $\rho = 1.3$ g cm^{-3}. With $C = 16$, Eqs. (8), (9), and (10) give

$$\varepsilon_{s,r} = 2.4, \tag{11a}$$

and

$$\tan \delta_s = 0.0059[1.38 \exp(-\beta E_0/k_B T)], \tag{11b}$$

where the factor 1.38 ensures that the term in brackets equals 1 at $T = 298$ K. By Eq. (1), a sample consisting purely of this model substance would have $\alpha = 0.04$ dB/m at 50 MHz and 273 K.

This modeling could be improved by laboratory investigations of candidate materials over a range of temperatures and frequencies. Systematic data are not available for plausible materials at temperatures below 273 K in the frequency range 10 to 100 MHz. Complex permittivities have been measured for several salt-containing ices over the range 193 to 271 K at 5 GHz (Matsuoka *et al.* 1997; see also Matsuoka *et al.* 1996). This type of systematic laboratory exploration is badly needed for the frequencies appropriate to Europa radar sounding. When such data become available, the simulations described here should be reexamined.

Nevertheless, it is encouraging that the values in Eqs. (11) are similar to those found for many other natural Solar System materials. The surfaces of Mars and Mercury have values for ε_r between 1.5 and 3 and loss tangents of about 0.005 (Olhoeft and Strangway 1975). At room temperature, terrestrial rock powders with densities of 1 g cm^{-3} have typical values for ε_r of about 2 and tan δ about 0.005. Terrestrial rocks have ε_r in the range 2 to 10 and tan δ in the range 10^{-3} to 10^{-1}, with a typical value tan $\delta \approx 0.04$. Meteorites with negligible metallic iron content are electrically similar to rocks (Campbell and Ulrichs 1969). These materials then have α approaching 0.1 dB/m. Terrestrial dry salt deposits have $\alpha \approx 0.01$ dB/m (Unterberger 1978, Daniels *et al.* 1988), a lower attenuation than that given by Eqs. (11), so that modeling ice impurities on Europa as terrestrial salt deposits would give deeper possible sounding depths than those found here.

Globally averaged impurity concentrations in ice at Europa's surface of more than a few weight percent of dark material appeared unlikely due to the strength of ice absorption bands in reflection spectra (Clark *et al.* 1986). Of course, there is no guarantee that impurity concentrations are not higher at depth. However, recent data from the Galileo near-infrared mapping spectrometer (McCord *et al.* 1998) suggest that particular regions of the surface have substantially higher impurity concentrations in the form of hydrated salt minerals.

Results for $f = 0.01$, 0.1, and 0.5, using Eqs. (1), (7), and (11), are shown in Fig. 2. At low temperatures where α is dominated by impurities in the ice, and provided that the imaginary parts of the permittivities are much smaller than the real parts (true for the materials considered here), Eqs. (1) and (7) give $\alpha \propto f \tan \delta_s \propto f\varepsilon_{s,i}$ for $f \ll 1$. The results of Fig. 2 may be accordingly scaled for different choices of f, C, ρ, or tan δ_s.

We have assumed that impurities are mixed intimately throughout Europa's ice. This could be an appropriate model for material emplaced via erupting plumes, for example. However, other possibilities can be envisioned. If briny ice erupts and flows onto Europa's surface, then as the ice freezes, dissolved salts will be concentrated into an unfrozen layer. As the temperature continues to drop, this layer would eventually freeze entirely, yielding a boundary between two media of different permittivities rather than an intimate mixture. Further experimental and modeling work will be required to determine the attenuation properties of these more complex geometries. We caution that some terrestrial samples, such as permafrost at 263 K, show much more complex dielectric behavior as a function of frequency (Olhoeft 1977) than the simple physical mixtures modeled here.

Ambiguities in radar sounding of the Filchner–Ronne ice shelf in Antarctica provide an additional caution. The origin of a radar sounding horizon at a depth of 170 m had been identified as due either to an internal reflecting horizon within the ice or as a surprisingly shallow base of the ice shelf, with the latter explanation being preferred (Robin *et al.* 1983). Direct drilling subsequently demonstrated that below the horizon at 170 m was another 295 m of ice (Engelhardt and Determann 1987). The lowest 35 m of ice appeared to be slush. The observed reflection was evidently due to an internal horizon, probably resulting from an underlying layer of basal sea ice (Engelhardt and Determann 1987, Jenkins and Doake 1991).

V. TEMPERATURE PROFILES OF EUROPA'S ICE LAYER

Since attenuation in ice is strongly temperature dependent, the temperature profile of Europa's ice layer is important for modeling attenuation with depth. Because we wish to examine radar sounding for ice layers of varying thickness, our approach is to choose a candidate ice layer thickness, set the temperatures at the top and bottom of this layer, and determine the required temperature profile throughout the layer. Radar attenuation can then be calculated by convolving this temperature profile with attenuation as a function of temperature.

Europa's surface-averaged temperature is 100 K, with mean surface temperatures as low as 50 K at the poles. Voyager and Galileo observations give a Europan equatorial evening terminator temperature of about 90 K and a subsolar brightness temperature of 128 K (Orton *et al.* 1996). A reexamination of the solid-state greenhouse effect on Europa (Urquhart and Jakosky 1996) gives average surface temperatures of 93–94 K with greenhouse warmings of 0 to 10 K. Ojakangas and Stevenson (1989) calculated average solar temperatures for Europa as a function of latitude, taking into account Europa's obliquity. They found a surface-averaged temperature of 100 K, with mean surface temperatures varying from 110 K at the equator to 52 K at the poles. We take the temperature at the base of the ice to be the melting temperature of ice at the pressure appropriate to that depth, ignoring possible effects due to incorporated salts. The former is a minor effect; for Europan surface gravity of 1.3 m s^{-2}, the Clapeyron equation gives a melting temperature at 100 km depth of 263 K.

Heat Loss by Conduction

For ice shell thicknesses less than ~30 km, Squyres *et al.* (1983) argued that subsolidus convection would not occur within Europa's ice, so that heat loss would be due to conduction. In this case, the equilibrium temperature profile is, to a good approximation, determined by solving the one-dimensional time-independent thermal diffusion equation

$$\frac{d}{dz}\left(\kappa\frac{dT}{dz}\right) = -q, \tag{12}$$

where z is the depth below the surface, κ is the thermal conductivity of ice, and q is the volumetric heat dissipation rate due to tidal heating of the ice layer.

Were κ constant and $q \approx 0$, Eq. (12) would yield the simple linear temperature profile

$$T(z) = T_s + (T_b - T_s)z/b, \tag{13}$$

where T_s and T_b are the temperatures at the surface and base of the ice layer, respectively, and b is the thickness of the ice layer. However, the temperature dependence of the thermal conductivity of ice is well-known,

$$\kappa(T) = a/T + c, \tag{14}$$

where $a = 4.88 \times 10^7$ erg cm^{-1} s^{-1} and $c = 4.68 \times 10^4$ erg cm^{-1} s^{-1} K^{-1} (Hobbs 1974). Moreover, we are interested in the case where tidal heating in the ice shell maintains a liquid ocean, so that q cannot equal 0. For temperatures below $\sim 10^3$ K, $\kappa(T) \approx a/T$. Most investigations of tidal heating in Europa's ice shell have taken q to be constant throughout the shell (Cassen *et al.* 1979, 1980, 1982, Squyres *et al.* 1983, Ross and Schubert 1987). In this case, solving Eq. (12) gives

$$T(z) = T_s \exp[(H + qb)z/a - qz^2/2a], \tag{15}$$

where $H = \kappa(dT/dz)_b$ is the heat flow into the ice shell from the ocean, due to heat flow from Europa's core. For the special case where $H = 0$, $T(z)$ is determined uniquely in terms of b, T_s, and T_b as

$$T(z) = T_s \exp[(2z - z^2/b)/s], \tag{16}$$

where $s = b/\ln(T_b/T_s) = 2a/bq$.

However, for realistic ice rheologies, q is extremely temperature dependent and the assumption of constant q is extremely invalid. For both the Maxwell and the Glen flow rheologies, $q \propto \exp[l(1 - T_m/T)]$, where T_m is the melting temperature. For the Maxwell rheology, we take l to vary linearly from $l = 15$ at 100 K to $l = 24$ at T_m. For the Glen's flow rheology, $l \approx 61$ (Ojakangas and Stevenson 1989). For the Maxwell rheology, q increases by ~12 orders of magnitude between 100 and 273 K, and by a factor ~10 between 250 and 273 K.

Realistic solutions of Eq. (12) must take q to be strongly peaked near the bottom of the ice layer, where the ice is warm. Ojakangas and Stevenson (1989) solve Eq. (12) to determine b, given H, q, T_b, and T_s. Here we choose b, T_s, and T_b and solve for $T(z)$. Equation (12) may be rewritten as

$$(dy/dz)\, d(dy/dz) = -q(T)\, dy/a, \tag{17}$$

where $y \equiv \ln(T)$. Integrating from z to b gives

$$[1/T(z)](dT/dz) = (H/a)^2 + (2/a)I(T_b), \tag{18}$$

where the approximation

$$\int_{Tz}^{T_b} [q(T)/T]\, dT \approx \int_0^{T_b} [q(T)/T]\, dT \equiv I(T_b) \tag{19}$$

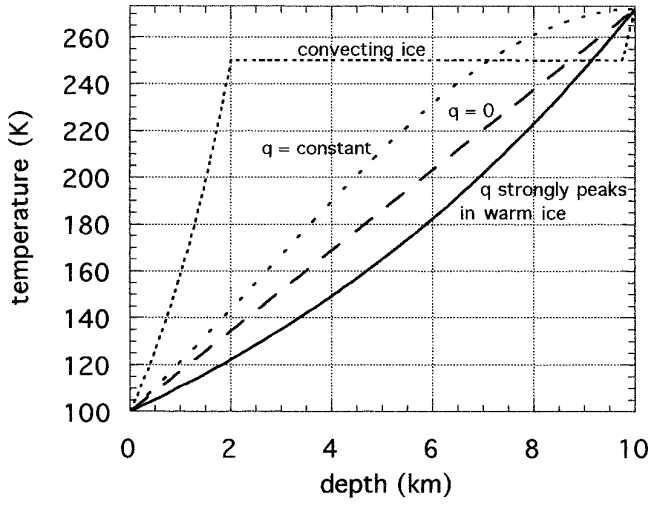

FIG. 3. Illustrative examples of temperature profiles in Europa's ice (assuming the ice layer to be 10 km thick) for convecting and conducting subsurface models, and different assumptions about the volumetric heating rate q. The curve labeled "convecting ice" assumes a 2-km-thick conducting lithosphere underlain by a 7.75-km-thick convecting region at 250 K. This region is in turn underlain by a 250-m-thick conducting boundary layer. The remaining curves assume an entirely conducting ice shell. The dashed line corresponds to $q = 0$ (Eq. (13)), the dotted line assumes that q is constant throughout the ice (Eq. (16)), and the solid line assumes that q strongly peaks in the warm ice (Eq. (20)). Of the conducting models, only the latter is consistent with realistic ice rheologies.

holds provided $q(T)$ is sufficiently strongly peaked as T approaches T_b. Integrating Eq. (18) from z to b and requiring $T = T_s$ at $z = 0$ gives the approximate solution

$$T(z) = T_s \exp(z/h), \tag{20}$$

where $h = b/\ln(T_b/T_s)$ and

$$\ln(T_b/T_s) = (b/a)[H^2 + 2aI(T_b)]^{1/2}. \tag{21}$$

For $T_b = 273$ K, $T_s = 100$ K, and $b = 20$ km, $[H^2 + 2aI(T_b)]^{1/2} \equiv A(b) = 25$ erg cm^{-2} s^{-1}.

This may be checked for consistency with the results of Ojakangas and Stevenson (1989), who found, for example, that for $H = 10$ erg cm^{-2} s^{-1} (about that due to the radiogenic heating expected from a chondritic Europa core) and total tidal dissipation (for a Maxwell rheology) in the ice shell $dE/dt = 2 \times 10^{18}$ erg s^{-1}, the average ice thickness $b = 21$ km. Defining the flux $F = (dE/dt)/4\pi r_e^2$, where r_e is Europa's radius, we have $I(T_b) \approx F/b$, giving $A(b) \approx 21$ erg cm^{-2} s^{-1}. The temperature profiles $T(z)$ for Eqs. (13), (15), and (20) are illustrated in Fig. 3.

Ojakangas and Stevenson (1989) find that the ice thickness b derived in their model is sensitive at only the 10% level to the different choices $H = 10$ erg cm^{-2} s^{-1} or $H = 0$. However, in models that take into account both radiogenic and tidal heating of Europa's core, H may be higher. Squyres *et al.* (1983) calculated $H \approx 24$ erg cm^{-2} s^{-1}. We may use Eq. (21) to derive an approximate expression for b given dE/dt and H. This expression will be useful in calculating boundary layer thickness in the convecting ice case, discussed in the next section. Using $I(T_b) \approx F/b$, Eq. (21) may be solved for b, giving

$$b \approx (a/2H^2)[-2F \pm (4F^2 + 4H^2[\ln(T_b/T_s)]^2)^{1/2}]. \tag{22}$$

For $H = 10$ and 24 erg cm^{-2} s^{-1}, Eq. (22) gives $b \approx 26$ and 15 km, respectively.

Preliminary Convective Models

There is suspicion that heat loss through at least some of Europa's ice shell is by convection rather than conduction (Pappalardo *et al.* 1998). Modeling of these processes remains at a preliminary stage (McKinnon 1997b, Pappalardo *et al.* 1998, Rathbun *et al.* 1998), so estimates of internal temperature gradients appropriate to convection are likely to prove premature. Nevertheless, because of the possible importance of such models, we examine preliminary ones here, recognizing that further work will be required as these models mature.

The thermal structure for a convecting icy satellite mantle may be summarized as follows (Mueller and McKinnon 1988, McKinnon 1998). The uppermost ice layer forms a rigid conducting lid, through which heat is lost by conduction. Below this lid lies a comparatively thin boundary layer, under which lies the convecting ice mantle. The temperature gradient through the convecting mantle is adiabatic and in fact is nearly isothermal. Below the convecting layer lies a final thin conducting boundary layer. Pappalardo *et al.* (1998) propose a convective model for Europa's ice consisting of a conducting layer $\lesssim$2 km thick underlain by a convecting layer between 2 and 8 km thick. This convecting layer would in turn be underlain by a thin boundary layer, underneath which would lie the putative Europan ocean. The average temperature of the convecting layer at the onset of convection was taken to be $\sim$235 K. McKinnon (1997b) suggests that the convecting layer's temperature might be as high as 250 K.

As preliminary models to use for radar sounding simulations, we adopt the following thermal structure. We extend the temperature gradient down from the surface at 100 K through the brittle lithosphere and the thin upper boundary layer to a depth of 2 km, where the temperature reaches either 235 or 250 K. (The temperature of this convecting layer will be the key limitation on radar penetration.) The temperature remains at either 235 or 250 K down through an isothermal convecting depth that we vary from 1 to 8 km thickness. The convecting layer is underlain by a

boundary layer of thickness δ, through which the temperature increases from 235 or 250 K to the melting point of water corresponding to the given depth. Since both the upper and the lower boundary layers are being tidally heated (the bottom layer much more so!), the temperature gradient through these layers is not linear, but is rather given by Eq. (20), with T_b and T_s corresponding to the temperatures at the bottom and top of the boundary.

Were the lower boundary layer heated only from below, as in typical convection models (Mueller and McKinnon 1988), we could calculate its thickness simply via $\delta = \kappa \Delta T / F$, where ΔT is the temperature drop across the boundary (Stevenson *et al.* 1983). However, the situation is complicated by the fact that most of the tidal dissipation in Europa's ice shell will take place within this lower boundary layer, where the ice is warmest. We may therefore approximate the thickness of this boundary layer by using Eq. (22), with $T_b \approx 272$ K, $T_s = 250$ K, and b being taken as the boundary layer thickness δ. For H ranging from 10 to 24 erg cm^{-2} s^{-1}, $\delta \approx 250$ m. For the case where the total ice thickness is 10 km, the resulting subsurface temperature distribution is contrasted with conducting ice models in Fig. 3. If the temperature of the convecting layer is instead taken to be 235 K, $\delta \approx 750$ m for both $H = 10$ and 24 erg cm^{-2} s^{-1}.

VI. SOUNDING DEPTHS IN EUROPAN ICE

For $T(z)$ given by Eq. (20), Fig. 4 shows the two-way attenuation of 50 MHz radar propagating into 10 km of dirty ice underlain by an ocean at 272 K for surface temperatures of 100 and 50 K. The effect of impurities mixed in with the ice is shown by letting f vary from 0.01 to 0.5. Two-way attenuations through the ice are 35–55 dB for $f = 0.01$. Figure 5 shows total two-way attenuations for analogous dirty ice layers, for thicknesses varying from 0 to 20 km. Figure 6 shows total two-way attenuations for convecting dirty ice models, for ice thicknesses varying from 3 to 20 km.

The radar equation may be written (Gudmansen 1971)

$$\frac{P_r}{P_t} = \frac{G^2 \lambda^2 L_{vi}^2 L_{iw} g_r}{(4\pi)^2 [2(h_a + b)]^2 L_{2i}}, \tag{23}$$

where P_r and P_t are the received and transmitted power at the antenna, G is the gain, λ is the free-space transmission wavelength, L_{vi} is the power transmission factor at the vacuum–ice interface, L_{iw} is the power reflection coefficient at the ice–water or ice–bedrock interface (which we assume to be smooth at the scale of the observing wavelength), g_r is the refractive gain, h_a is the spacecraft orbital altitude, b is the thickness of the ice layer, and L_{2i} is the two-way dielectric absorption of the dirty ice. The minimum

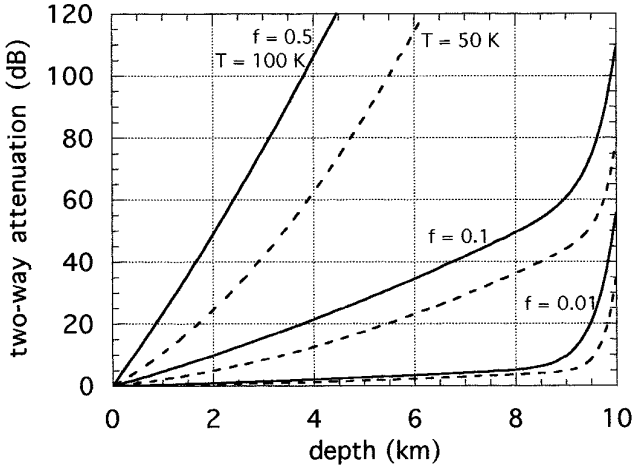

FIG. 4. Two-way attenuation in dirty Europan ice for a 10-km-thick conducting ice layer underlain by liquid water with $T(z)$ given by Eq. (20). Solid and dashed line pairs assume $T_s = 100$ and 50 K, respectively. From bottom to top, line pairs assume successive mixing fractions $f = 0.01$, 0.1, and 0.5.

detectable power is the noise power of the receiver, so we set $P_r = k_B T_n B(S/N)$, where $T_n \approx 5 \times 10^4$ K is the jovian radio noise temperature at Europa (Carr *et al.* 1983), B is the bandwidth, and S/N is the signal-to-noise ratio. We can determine the dielectric absorption of the dirty ice layer that can be tolerated and still allow detection of a Europan ocean by solving Eq. (23) for L_{2i} for appropriate choices of the other parameters.

For definiteness, we choose an RF bandwidth $B = 2$ MHz, giving a range resolution of $c/2Bn \approx 40$ m, where the index of refraction $n \approx 1.77$ for ice at Europan temperatures. We take the effective peak power of the antenna to

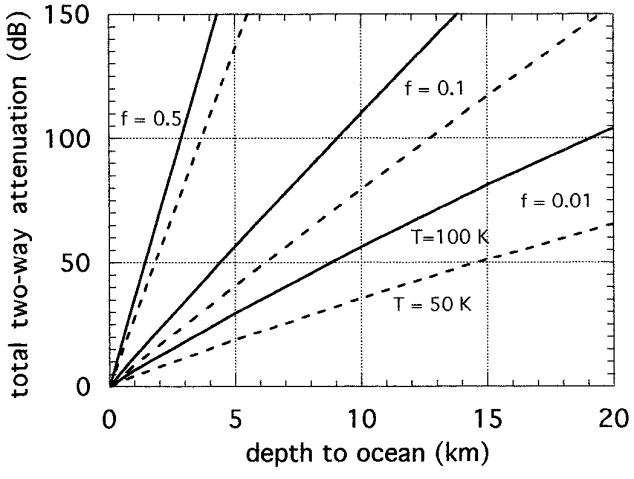

FIG. 5. Total two-way attenuation for conducting dirty ice thicknesses varying from 0 to 20 km. Solid and dashed lines correspond to the same values of T_s and f as in Fig. 4.

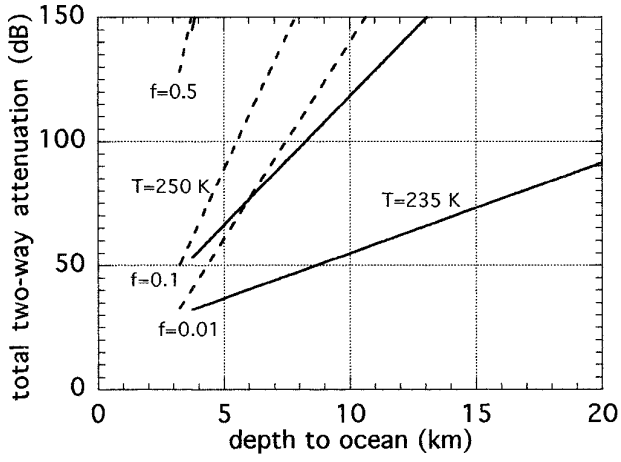

FIG. 6. Total two-way attenuation for convecting dirty ice on Europa. The models assume a 2-km-thick brittle conducting lithosphere underlain by a convecting ice layer from 1 to 18 km thick, in turn underlain by a thin conducting boundary layer. Each set of curves is labeled by an impurity mixing fraction *f*. Solid lines correspond to convecting ice at 235 K; dashed lines correspond to similar models in which the convecting ice has a temperature of 250 K.

be $P_t = 300$ W. One scenario for achieving this peak power is to transmit frequency modulated pulses of 150-μs duration at a 600-Hz repetition rate. By processing the return signal the individual modulations within each 150-μs duration pulse can be combined and an effective peak power of 300 W can be achieved with an average power of only 2 W. (In comparison, 10 m^2 of GaAs solar arrays at Europa's heliocentric distance, if undegraded by radiation, would provide 100 W of power.) The individual pulses can then be combined (180 pulses per bin) to give a 0.3-s period for sampling the surface.

We set $S/N = 1$ and $G = 10$ dB. At $\lambda = 6$ m, $\varepsilon_r \approx 3.1$ for 100 K ice, giving $L_{vi} \approx -0.3$ dB. Reflection loss at an ice/bedrock interface would be -10 to -20 dB, whereas loss at an ice/water interface $L_{iw} \approx -1$ dB and therefore distinguishable from an ice/rock interface (Evans and Smith 1969, Gudmansen 1971). The refraction gain for $h_a + b \approx 100$ km is $g_r \approx 2$ dB (Gudmansen 1971). Equation (23) then gives 20 log $(h_a + b)$ + 10 log $(L_{2i}) \approx 151$ dB. For $h_a = 100$ km, $L_{2i} \approx 53$ dB, varying slightly with b. Even taking into account system noise and requiring $S/N \approx 20$ dB, a realistic system could possibly improve over this result by ~30 dB through pulse compression and coherent summation of individual pulses. Doppler filtering can be used to reduce the along-track spatial extent of the sampled area. By frequency filtering the returned signal, returns originating from the surface in front or behind the spacecraft can be removed. By this method a spot size of roughly 1 km (from an orbit altitude of 100 km) can be obtained in the along-track direction.

For a realistic orbiting radar at 100 km altitude, an ice/ocean interface can be imaged to a depth of ~10 km (15 km at the poles) for conducting ice with 1% lunar soil impurities. For impurities at the 10% mixing level, an ice/ocean interface could be detected ~5 km down. Even for impurities at the 50% level, detection could be achieved at depths of 1 to 2 km. In general, deeper sounding is favored by moving poleward; however, ice thickness is also expected to increase, on average, at high latitudes (Ojakangas and Stevenson 1989).

In the convecting case, an ice/ocean interface could be imaged to a depth ~10 km for ice containing 1% impurities, if the convecting layer were at a temperature ~235 K. Increasing this temperature to 250 K reduces the depth to which an ice/water interface could be imaged to ~5 km. Impurities at the 10% level allow detections to depths ~3–5 km. Convecting ice at 250 K containing impurities at the 50% level will show considerable attenuation with depth. An uncertainty in all these results remains the absence of experimental values for the imaginary permittivity of ice at low temperatures in the frequency range 10 to 100 MHz.

If liquid water exists within several kilometers of Europa's surface, as suggested by some interpretations of recent Galileo images (McKinnon 1997a, Carr *et al.* 1998), our calculations suggest that a radar at 100 km altitude should be able to detect it. Nevertheless, potential major uncertainties, difficult to quantify, remain in predicting radar detectability of a Europan ocean and in interpreting actual sounding data. These include scattering from subsurface heterogeneities, ambiguous reflections from internal ice horizons, liquid brine inclusions, and the geometrical configuration of ice–water interfaces. Only performing the experiment at Europa will test these uncertainties.

ACKNOWLEDGMENTS

We acknowledge helpful conversations with R. Lorenz, R. Pappalardo, W. B. McKinnon, Xuan-Min Shao, and D. Holden and careful reviews by G. Pettengill and an anonymous referee. C.F.C. acknowledges support from the NASA exobiology program and a Presidential Early Career Award for Scientists and Engineers. Part of this research was conducted at the Jet Propulsion Laboratory, California Institute of Technology, with support from NASA.

REFERENCES

Bada, J. L., C. Bigham, and S. L. Miller 1994. Impact melting of frozen oceans on the early Earth: Implications for the origin of life. *Proc. Natl. Acad. Sci. USA* **91,** 1248–1250.

Belton, M. J. S., and 33 colleagues 1996. Galileo's first images of Jupiter and the Galilean satellites. *Science* **274,** 377–385.

Black, G. J., D. B. Campbell, and S. J. Ostro 1996. The icy Galilean satellites: 70 cm wavelength radar properties. *Lunar Planet. Sci. Conf. 27th*, 121.

Bussey, H. E. 1979. Microwave dielectric measurements of lunar soil with a coaxial line resonator method. *Proc. Lunar Planet. Sci. Conf. 10th*, 2175–2182.

Campbell, M. J., and J. Ulrichs 1969. Electrical properties of rocks and their signifance for lunar radar observations. *J. Geophys. Res.* **74,** 5867–5881.

Carr, M. H., M. J. S. Belton, C. R. Chapman, M. E. Davies, P. Geissler, R. Greenberg, A. S. McEwen, B. R. Tufts, R. Greeley, R. Sullivan, J. W. Head, R. T. Pappalardo, K. P. Klaasen, T. V. Johnson, J. Kaufman, D. Senske, J. Moore, G. Neukum, G. Schubert, J. A. Burns, P. Thomas, and J. Veverka 1998. Evidence for a subsurface ocean on Europa. *Nature* **391,** 363–365.

Carr, T. D., M. D. Desch, and J. K. Alexander 1983. Phenomenology of magnetospheric radio emissions. In *Physics of the Jovian Magnetosphere* (A. J. Dessler, Ed.), pp. 226–284. Cambridge Univ. Press, Cambridge.

Cassen, P., R. T. Reynolds, and S. J. Peale 1979. Is there liquid water on Europa? *Geophys. Res. Lett.* **6,** 731–734.

Cassen, P., S. J. Peale, and R. T. Reynolds 1980. Tidal dissipation in Europa: A correction. *Geophys. Res. Lett.* **7,** 987–988.

Cassen, P., S. J. Peale, and R. T. Reynolds 1982. Structure and thermal evolution of the Galilean satellites. In *Satellites of Jupiter* (D. Morrison, Ed.), pp. 93–128. Univ. of Arizona Press, Tucson.

Chung D. H., and W. B. Westphal 1973. Dielectric spectra of Apollo 15 and 16 lunar solid samples. *Proc. Fourth Lunar Sci. Conf.* **3,** 3077–3091.

Chung, D. H., W. B. Westphal, and G. R. Olhoeft 1972. Dielectric properties of Apollo 14 lunar samples. *Proc. Third Lunar Sci. Conf.* **3,** 3161–3172.

Chyba, C. F., and G. D. McDonald 1995. The origin of life in the Solar System: Current issues. *Annu. Rev. Earth Planet. Sci.* **23,** 215–249.

Clark, R. N., F. P. Fanale, and M. J. Gaffey 1986. Surface composition of natural satellites. In *Satellites* (J. A. Burns and M. S. Matthews, Eds.), pp. 437–491. Univ. of Arizona Press, Tucson.

Daniels, D. J., D. J. Gunton, and H. F. Scott 1988. Introduction to subsurface radar. *IEEE Proc.* **135,** 278–320.

Drewry, D. J. 1981. Radio echo sounding of ice masses: Principles and applications. In *Remote Sensing in Meteorology, Oceanography and Hydrology* (A. P. Cracknell, Ed.), pp. 270–284. Wiley, New York.

Engelhardt, H., and J. Determann 1987. Borehole evidence for a thick layer of basal ice in the central Ronne Ice Shelf. *Nature* **327,** 318–319.

Evans, S. 1965. Dielectric properties of ice and snow—A review. *J. Glaciol.* **5,** 773–792.

Evans, S., and B. M. E. Smith 1969. A radio echo equipment for depth sounding in polar ice sheets. *J. Sci. Instr.* **2,** 131–136.

Fisher, E., G. A. McMechan, M. R. Gorman, A. P. R. Cooper, C. L. V. Aiken, M. E. Ander, and M. A. Zumberge 1989. Determination of bedrock topography beneath the Greenland ice sheet by three-dimensional imaging of radar sounding data. *J. Geophys. Res.* **94,** 2874–2882.

Gough, S. R. 1972. A low temperature dielectric cell and the permittivity of hexagonal ice to 2 K. *Can. J. Chem.* **50,** 3046–3051.

Gudmansen, P. 1971. Electromagnetic probing of ice. In *Electromagnetic Probing in Geophysics* (J. Wait, Ed.), pp. 321–348. Golem Press, Boulder, CO.

Hallikainen, M., and D. P. Winebrenner 1992. The physical basis for sea ice remote sensing. In *Microwave Remote Sensing of Sea Ice*, Monoraph 68, pp. 29–46. American Geophysicist Union.

Hobbs, P. V. 1974. *Ice Physics*, Clarendon Press, Oxford.

Jenkins, A., and C. S. M. Doake 1991. Ice–ocean interaction on Ronne Ice Shelf, Antarctica. *J. Geophys. Res.* **96,** 791–813.

Johari, G. P., and P. A. Charette 1975. The permittivity and attenuation in polycrystalline and single-crystal ice Ih at 35 and 60 MHz. *J. Glaciol.* **14,** 293–303.

Johari, G. P., and S. J. Jones 1978. The orientation polarization in hexagonal ice parallel and perpendicular to the c-axis. *J. Glaciol.* **21,** 259–276.

Kapitsa, A. P., J. K. Ridley, G. de Q. Robin, M. J. Siegert, and I. A. Zotikov 1996. A large deep freshwater lake beneath the ice of central East Antarctica. *Nature* **381,** 684–686.

Kargel, J. S. 1991. Brine volcanism and the interior structures of asteroids and icy satellites. *Icarus* **94,** 368–390.

Kawada, S. 1978. Dielectric anisotropy of Ice Ih. *J. Phys. Soc. Jpn.* **44,** 1881–1886.

Kovacs, A., and R. M. Morey 1992. Estimating sea ice thickness from impulse radar sounding time of flight data. In *Ground Penetrating Radar* (J. Pilon, Ed.), Paper 90-4, pp. 117–124. Geological Survey Canada.

Lamb, J., and A. Turney 1949. The dielectric properties of ice at 1.25 cm wavelength. *Proc. Phys. Soc. London B* **62,** 272–273.

Malin, M. C., and D. C. Pieri 1986. Europa. In *Satellites* (J. A. Burns and M. S. Matthews, Eds.), pp. 689–717. Univ. of Arizona Press, Tucson.

Matsuoka, T., S. Fujita, and S. Mae 1996. Effect of temperature on dielectric properties of ice in the range 5–39 GHz. *J. Appl. Phys.* **80,** 5884–5890.

Matsuoka, T., S. Fujita, and S. Mae 1997. Dielectric properties of ice containing ionic impurities at microwave frequencies. *J. Phys. Chem.* B **101,** 6219–6222.

Mätzler, C., and U. Wegmüller 1987. Dielectric properties of fresh-water ice at microwave frequencies. *J. Phys.* D **20,** 1623–1630.

McCord, T. B., G. B. Hansen, F. P. Fanale, R. W. Carlson, D. L. Matson, T. V. Johnson, W. D. Smythe, J. K. Crowley, P. D. Martin, A. Ocampo, C. A. Hibbitts, J. C. Granahan, and the NIMS team 1998. Salts on Europa's surface detected by Galileo's Near Infrared Mapping Spectrometer, *Science* **280,** 1242–1245.

McKinnon, W. B. 1997a. Sighting the seas of Europa. *Nature* **386,** 765–766.

McKinnon, W. B. 1997b. Convective instabilities in Europa's floating ice shell. *Bull. Am. Astron. Soc.* **29,** 984.

McKinnon, W. B. 1998. Geodynamics of icy satellites. In *Solar System Ices* (B. Schmitt *et al.*, Eds.), pp. 525–550. Kluwer Academic, The Netherlands.

Mueller, S., and W. B. McKinnon 1988. Three-layered models of Ganymede and Callisto: Compositions, structures, and aspects of evolution. *Icarus* **76,** 437–464.

Nielsen, L. E. 1978. *Predicting the Properties of Mixtures: Mixture Rules in Science and Engineering*. Dekker, New York.

Ojakangas, G. W., and D. J. Stevenson 1989. Thermal state of an ice shell on Europa. *Icarus* **81,** 220–241.

Olhoeft, G. R. 1977. Electrical properties of natural clay permafrost. *Can. J. Earth Sci.* **14,** 16–24.

Olhoeft, G. R., and D. W. Strangway 1975. Dielectric properties of the first 100 meters of the Moon. *Earth Planet. Sci. Lett.* **24,** 394–404.

Olhoeft, G. R., A. L. Frisillo, and D. W. Strangway 1974. Electrical properties of lunar soil sample 15301,38. *J. Geophys. Res.* **79,** 1599–1604.

Orton, G. S., J. R. Spencer, L. D. Travis, T. Z. Martin, and L. K. Tamppari 1996. Galileo photopolarimeter–radiometer observations of Jupiter and the Galilean satellites. *Science* **274,** 389–391.

Ostro, S. J. 1982. Radar properties of Europa, Ganymede, and Callisto. In *Satellites of Jupiter* (D. Morrison, Ed.), pp. 213–236. Univ. of Arizona Press.

Ostro, S. J., and E. M. Shoemaker 1990. The extraordinary radar echoes from Europa, Ganymede, and Callisto: A geological perspective. *Icarus* **85,** 335–345.

Ostro, S. J., and 11 colleagues 1992. Europa, Ganymede, and Callisto:

New radar results from Arecibo and Goldstone. *J. Geophys. Res.* **97,** 18,227–18,244.

Oswald, G. K. A. 1975. Investigation of sub-ice bedrock characteristics by radio-echo sounding. *J. Glaciol.* **14,** 75–87.

Oswald, G. K. A., and G. de Q. Robin 1973. Lakes beneath the antarctic ice sheet. *Nature* **245,** 251–254.

Pappalardo, R. T., J. W. Head, R. Greeley, R. J. Sullivan, C. Pilcher, G. Schubert, W. B. Moore, M. H. Carr, J. M. Moore, M. J. S. Belton, and D. L. Goldsby 1998. Geological evidence for solid-state convection in Europa's ice shell. *Nature* **391,** 365–368.

Paterson, W. S. B., and J. C. Savage 1970. Excess pressure observed in a water-filled cavity in Athabasca glacier. *Can. J. Glaciol.* **9,** 103–107.

Rathbun, J. A., G. S. Musser, and S. W. Squyres 1998. Thermal-mechanical properties of possible ice diapirs on Europa. *Lunar Plan. Sci. Conf. 29th*, 1087–1088.

Reynolds, R. T., S. W. Squyres, D. S. Colburn, and C. P. McKay 1983. On the habitability of Europa. *Icarus* **56,** 246–254.

Reynolds, R. T., C. P. McKay, and J. F. Kasting 1987. Europa, tidally heated oceans, and habitable zones around giant planets. *Adv. Space Res.* **7**(5), 125–132.

Robin, G. de Q., C. S. M. Doake, H. Kohnen, R. D. Crabtree, S. R. Jordan, and D. Möller 1983. Regime of the Filchner-Ronne ice shelves, Antarctica. *Nature* **302,** 582–586.

Ross, M. N., and G. Schubert 1987. Tidal heating in an internal ocean model of Europa. *Nature* **325,** 133–134.

Saint-Amant, M., and D. W. Strangway 1970. Dielectric properties of dry, geologic materials. *Geophysics* **35,** 624–645.

Sihvola, A. H., and J. A. Kong 1988. Effective permittivity of dielectric mixtures. *IEEE Trans. Geosci. Remote Sens.* **26,** 420–429.

Sihvola, A. H., and J. A. Kong 1989. Correction to ''Effective permittivity of dielectric mixtures.'' *IEEE Trans. Geosci. Remote Sens.* **27,** 101–102.

Smith, B. A., and 21 colleagues 1979a. The Jupiter system through the eyes of Voyager 1. *Science* **204,** 951–972.

Smith, B. A., and 21 colleagues 1979b. The Galilean satellites and Jupiter: Voyager 2 imaging science results. *Science* **206,** 927–950.

Squyres, S. W. 1989. Prospects for the existence and detectability of an ocean on Europa. *Adv. Space Res.* **9**(2), 79–85.

Squyres, S. W., R. T. Reynolds, P. M. Cassen, and S. J. Peale 1983. Liquid water and active resurfacing on Europa. *Nature* **301,** 225–226.

Stevenson, D. J., T. Spohn, and G. Schubert 1983. Magnetism and thermal evolution of the terrestrial planets. *Icarus* **54,** 466–489.

Strangway, D. W., G. Simmons, G. LaTorraca, R. Watts, L. Bannister, R. Baker, J. D. Redman, and J. R. Rossiter 1974. Radio-frequency interferometry–A new technique for studying glaciers. *J. Glaciol.* **13,** 123–132.

Thompson, W. R., and S. W. Squyres 1990. Titan and other icy satellites: Dielectric properties of constituent materials and implications for radar sounding. *Icarus* **86,** 336–354.

Unterberger, R. R. 1978. Radar and sonar probing of salt. In *5th International Symposium on Salt*, pp. 423–437. Northern Ohio Geological Society.

Urquhart, M. L., and B. M. Jakosky 1996. Constraints on the solid-state greenhouse effect on the icy Galilean satellites. *J. Geophys. Res.* **101,** 21,169–21,176.

Warren, S. G. 1984. Optical constants of ice from the ultraviolet to the microwave. *Appl. Opt.* **23,** 1206–1225.

Watts, R. D., and A. W. England 1976. Radio-echo sounding of temperate glaciers: Ice properties and sounder design criteria. *J. Glaciol.* **17,** 39–48.

Wiik, H. B. 1956. The chemical composition of some stony meteorites. *Geochim. Cosmochim. Acta* **9,** 279–289.